ISSN 2035-911X

International Journal of
Energy & Technology
www.journal-enertech.eu

International Journal of Energy & Technology 2 (6) (2010) 1–11

UNSTEADY MIXED CONVECTION OF A MICROPOLAR FLUID IN A LID-DRIVEN CAVITY: EFFECTS OF DIFFERENT MICRO-GYRATION BOUNDARY CONDITIONS

Ali J. Chamkha[*], M.A. Mansour[o], Sameh E. Ahmed[**]

[*]Manufacturing Engineering Department, The Public Authority for Applied Education and Training, Shuweikh 70654, Kuwait, E-mail: achamkha@yahoo.com
[o]Department of Mathematics, Assuit University, Assuit, Egypt
[**]Department of Mathematics, South Valley University, Qena, Egypt, E-mail: sameh_sci_math@yahoo.com

ABSTRACT

In this work, a numerical solution of flow and heat transfer of a micropolar fluid in a lid-driven cavity under different micro-gyration boundary conditions is presented. A finite difference method is employed to solve the governing system of partial differential equations. The cases of strong concentration of microelement and weak concentration of microelement are considered. The effects of the governing parameters, namely the dimensionless time parameter, micro-gyration boundary conditions parameter and vortex viscosity parameter on the streamlines contours and temperature contours as well as the velocity profiles at the enclosure mid-section, angular velocity profiles at the enclosure mid-section, Nusselt number and average Nusselt number at the bottom and top walls of the enclosure are investigated. The results for the Newtonian fluid condition are validated by favorable comparisons with previously published results. The numerically results are shown graphically to illustrate special features of the solutions. The values of the average Nusselt number at the bottom and top walls of the enclosure are presented in tables.

Keywords: Lid-driven cavity; micropolar fluid; mixed convection; various boundary conditions

1. INTRODUCTION

Micropolar fluids are fluids of microstructure. They represent fluids consisting of rigid, randomly oriented or spherical particles suspended in a viscous medium, where the deformation of fluids particles is ignored (e.g. polymeric suspensions, animal blood, liquid crystals). In order to describe accurately the behavior of such fluids, the geometry and intrinsic motion of individual material particles have been taken into account, and the angular velocity field of rotation of particles and the conservation of the angular momentum are added in the theory of micropolar fluids by Eringen [1]. In this case, many classical concepts such as the symmetry of the stress tensor or absence of couple stresses are no longer existed. Owing to its relatively mathematical simplicity, the micropolar fluids model has been widely used in lubrication to investigate the polymer solutions in which the Newtonian lubricant is blended with small amount of long-chained additives. So far there have been many studies focusing on one-and two-dimensional non-Newtonian bearings by the micropolar fluids model [2-7]. For example, Abd-Elaziz and Ahmed [6] presented an analysis of unsteady boundary layer flow of a micropolar fluid near the rear stagnation point of a plane surface in a porous medium. The group method was used to solve this problem. It is found that, as the values of material parameter increase, the velocity distribution becomes more linear and as the permeability parameter increases, the velocity distribution assumes a more uniform shape within the boundary layer. A boundary layer analysis was presented by Mansour et al. [7] for combined heat and mass transfer characteristics of a micropolar fluid flowing past a vertical cylinder. These studies are examples for boundary layer flow but for internal flows there are little investigations in this field. Hsu and Hsu [8] presented a numerical study of natural convection of micropolar fluids in an enclosure with heat sources. Their numerical results indicate that the average Nusselt number is lower for a micropolar fluid, as compared to a Newtonian fluid. It is shown that high-powered heat source has negligible effect on the lower one's temperature, whereas it has significant effect on the higher one's temperature. Hsu and Wang [9] investigated the problem of mixed convection of micropolar fluids in a square cavity with a localized heat source. The flow in the cavity includes the externally induced stream at ambient temperature and the free flow induced by the heat source. The amount of microrotation in the cavity increases when the vortex viscosity increases. However, its value becomes lower as the spin gradient viscosity is increased.

Studies of the natural convection in Newtonian fluid inside the enclosures have received large attentions from researchers [10-17]. For Example, Abdul Hakeem et al [10] presented a numerical solution for the problem of Buoyancy convection in

a square cavity with mutually orthogonal heat generating baffles. The problem of effect of baffle–cavity ratios on buoyancy convection in a cavity with mutually orthogonal heated baffles was discussed by Kandaswamy et al. [11]. Bennacera et al. [12] presented a study of double diffusive convection in a vertical enclosure inserted with two saturated porous layers confining a fluid layer. On the other hand, the effect of an external oscillating sliding lid in driven cavity flows has received little research attention although it is important for understanding the transport phenomena in food processing applications, for example. Soh and Goodrich [18] outlined the basic transient flow features relevant to this problem using a time-accurate finite-difference scheme. Moreover, Iwatsu et al. [19] performed a numerical investigation on the effect of external excitation on the flow structure in a square cavity. Their results have shown similar flow structure to steady driven-cavity flows when utilizing small frequency values. Such a similarity, however, was noted to vanish when large frequency values were employed. A subsequent work by Iwatsu et al. [20] who carried out a numerical study of the viscous flow in a heated driven cavity under thermal stratification, where the oscillating lid was maintained at a higher temperature than the lower wall. Their results had revealed substantial enhancement in heat transfer rate at particular lid frequency values, which signals the presence of the resonance phenomena. From the above discussion and the survey of literature, it seems that the problem of mixed convection heat transfer in a cavity heated from below subjected to a sliding lid that exercises a mechanical oscillation has not been addressed yet. Such studies have been limited as discussed above to driven cavities under thermal stratification condition. Khanafer et al. [21] presented a numerical simulation of unsteady mixed convection in a driven cavity using an externally excited sliding lid. Their results show that the Reynolds number and Grashof number have a profound effect on the structure of fluid flow and heat transfer fields. As a matter of fact, their effects are associated with the direction of the sliding lid. Al-Amiri [22] used finite volume scheme to analyze the problem of momentum and energy transfer in a lid-driven cavity filled with a porous medium.

The main objective of this paper is to study unsteady mixed convection of a micropolar fluid in a lid-driven cavity under different micro-gyration boundary conditions. The governing equations of the problem are solved numerically using a finite difference method. The effects of governing parameters on flow and heat characteristics are investigated. The present results are compared for special cases with previously published work. The flow results are shown graphically while the values of average Nusselt number at the bottom and top walls of the enclosure are presented in tables.

2. GOVERNING EQUATIONS

Consider unsteady laminar mixed convection flow of a micropolar fluid in a square cavity with the physical dimensions given in Fig.1. In the present problem, the following assumptions have been made.

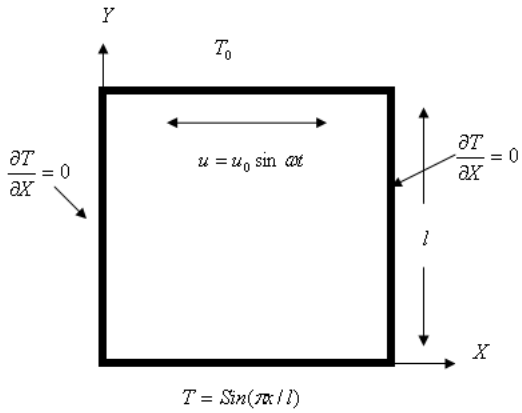

Figure 1. Flow configuration and coordinate system

a) The mechanically induced lid motion is assumed to oscillate with a velocity $u = u_0 \sin \omega t$ in the longitudinal direction.
b) The bottom wall of the cavity is non-uniformly heated.
c) Both of the case of strong concentration of microelement and weak concentration of microelement are considered.
d) The viscous, radiation and Joule heating effects are neglected.
e) The density is assumed to be a linear function of temperature [$\rho = \rho_0(1-\beta(T-T_0))$].

Under the above assumptions, the governing equations in dimensionless form can be written as:

$$\Omega = \frac{\partial V}{\partial X} - \frac{\partial U}{\partial Y} = -\nabla^2 \psi \tag{1}$$

$$\frac{\partial \Omega}{\partial \tau} + U\frac{\partial \Omega}{\partial X} + V\frac{\partial \Omega}{\partial Y} = \frac{1}{\mathrm{Re}}\left((1+\Delta)\nabla^2\Omega - \Delta\nabla^2 N\right) + \frac{Gr}{\mathrm{Re}^2}\frac{\partial \theta}{\partial X} \tag{2}$$

$$\frac{\partial N}{\partial \tau} + U\frac{\partial N}{\partial X} + V\frac{\partial N}{\partial Y} = \frac{\lambda}{\mathrm{Re}}\left(\frac{\partial^2 N}{\partial X^2} + \frac{\partial^2 N}{\partial Y^2}\right) + \frac{\Delta.B}{\mathrm{Re}}\left(\frac{\partial V}{\partial X} - \frac{\partial U}{\partial Y} - 2N\right) \tag{3}$$

$$\frac{\partial \theta}{\partial \tau} + U\frac{\partial \theta}{\partial X} + V\frac{\partial \theta}{\partial Y} = \frac{1}{\mathrm{Pr}\,\mathrm{Re}}\left(\frac{\partial^2 \theta}{\partial X^2} + \frac{\partial^2 \theta}{\partial Y^2}\right), \tag{4}$$

The dimensionless initial and boundary conditions are

$$\tau = 0:\ U = 1.0,\quad V = 0.0,\ \theta = 0.0,\ N = 0.0 \ \ everywhere$$
$$\tau > 0: U = V = \psi = 0,\quad \frac{\partial \theta}{\partial X} = 0,\quad N = \chi\frac{\partial V}{\partial X} \ \ at\ X = 0,1;\ 0 \le Y \le 1.0$$
$$\tau > 0: U = V = \psi = 0,\quad \theta = Sin(\pi X),\quad N = -\chi\frac{\partial U}{\partial Y} \ \ at\ Y = 0.0;\ 0 < X < 1.0$$
$$\tau > 0: U = Sin\varpi\tau,\ V = \psi = 0, \theta = 0,\quad N = -\chi\frac{\partial U}{\partial Y} \ \ at\ Y = 1.0;\ 0 < X < 1.0 \tag{5}$$

The boundary condition imposed on the vorticity is written as

$$\Omega_w = -\frac{\partial^2 \psi_w}{\partial S^2} \tag{6}$$

where w refers to the wall condition and n indicates the direction normal to the wall surface. It should be pointed out that the singularities in axial U velocity at the two upper corners are treated using a similar approaches reported in Ref.[23].

In the above equations, the following dimensionless variables are used.

$$\begin{gathered} X = \frac{x}{l},\ Y = \frac{y}{l},\ U = \frac{u}{u_0},\ V = \frac{v}{u_0},\ N = \frac{l}{u_0}\sigma, \psi = \frac{\Psi}{u_0 l}, \\ \tau = \frac{u_0 t}{l},\ \theta = \frac{T - T_0}{\Delta T},\ P = \frac{pl}{\mu u_0},\ \mathrm{Pr} = \frac{\upsilon}{\alpha},\ \mathrm{Re} = \frac{u_0 l}{\upsilon}, \Omega = \frac{l\zeta}{u_0}, \\ Gr = \frac{g\beta \Delta T l^3}{\upsilon^2},\ \Delta = \frac{k}{\mu},\ \chi = \frac{\gamma}{\mu j},\ B = \frac{l^2}{j},\ \Delta T = T_w - T_0, \end{gathered} \tag{7}$$

where all the parameters appearing in the above equations are given in the list of symbols

The heat transfer coefficients at the enclosure bottom and top walls in terms of the local Nusselt numbers are defined by

$$Nu_{b,T} = \left(\frac{-\partial \theta}{\partial Y} \right)_{Y=0,1}, \tag{8}$$

In addition, the average Nusselt number at the enclosure bottom and top walls are defined as

$$\overline{Nu_b} = \int_0^1 Nu_b dX, \tag{9}$$

$$\overline{Nu_T} = \int_0^1 Nu_T\, dX, \tag{10}$$

3. NUMERICAL METHOD

The numerical algorithm used to solve the dimensionless governing Eqs. (1)-(4) with the boundary conditions (5) is based on finite difference methodology. Central difference quotients were used to approximate the second derivatives in both the X- and Y-directions. The obtained discretized equations are then solved using the following algorithm.

a) Select a suitable grid. A grid 21×21 is a good start in many cases.
b) All dependent variables are initialized to zero.
c) The new boundary values at $(n+1)$ are calculated for all walls from the previous values at (n) .
d) The new temperature values at $(n+1)$ are calculated from previous (n) values at all internal grid points.
e) The vorticity , angular velocity and stream function are calculated in the same way as in step (d), respectively.
f) The velocity components U and V are calculated at $(n+1)$ from the values at (n) explicitly for all the internal grid points.
g) The same procedure is followed by starting with step (c) to obtain the solution at the next time step at $(n+2)$.
h) Test that τ less than maximum set time to finish the loop.
i) The Nusselt and average Nusselt numbers at the top and bottom walls are then calculated.

The numerical computations were carried out for (21×21) and ((31×31)grid nodal points with a time step of10^{-4} .

Table 1. Comparison of the average Nusselt number at the top wall between the present solution and other solutions

	$U_{\min}$	$U_{\max}$	Nu
Ref.[23]	-0.2122	1.0	2.01
Ref.[22]	-0.2037	1.0	1.94
Ref.[21]	-0.2093	1.0	2.02
Present	-0.2127264	1.0	2.086494

Khanafer et al. [21] used a finite-element scheme based on the Galerkin method of weighted residuals to solve the special case of this study which is the problem of mixed convection heat transfer in a lid driven cavity with uniform heat bottom wall ($\theta(X,0)=1.0$) but this method was found to be suitable and gave results that were very close to the numerical results obtained Khanafer et al. [21]. It can be seen from Figure 2 and Table 1 that the present results are in good agreement with those reported earlier by Khanafer et al. [21] when we apply the Khanafer et al. [21] model i.e Newtonian fluid $\Delta = 0$ and uniform heat bottom wall $\theta(X,0)=1.0$.

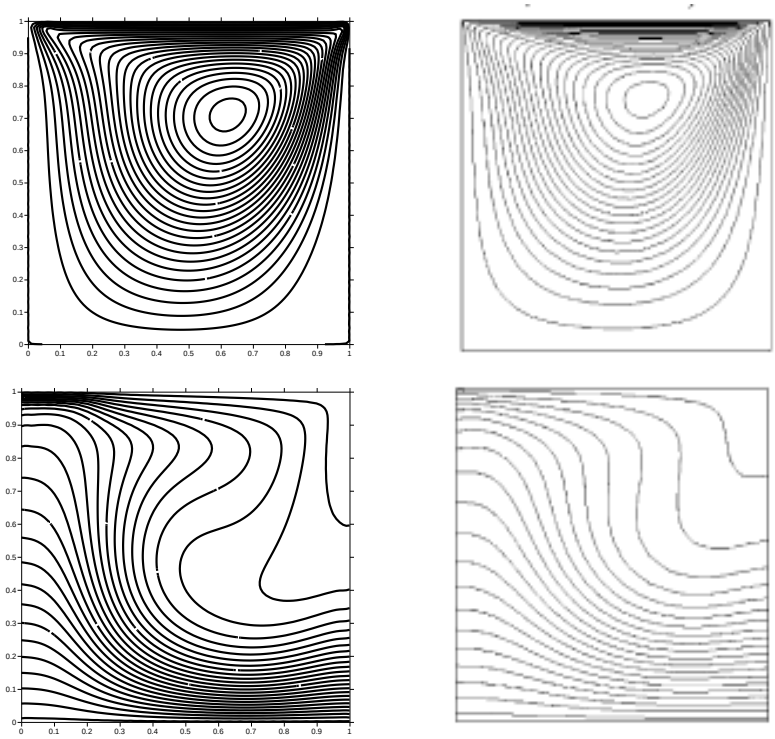

Figure 2. Comparisons between our results (left) and Khanafer et al. [21] (right). [Contours of streamlines (top) and contours of isotherms (bottom)]

4. RESULTS AND DISCUSSION

In this section, numerical results for the contours of the streamlines and temperature as well as selected velocity component, angular velocity component at the enclosure mid section, Nusselt number and average Nusselt number at the top and bottom walls of the enclosure for various values of the dimensionless time parameter τ , Reynolds number Re, micrograytion boundary condition parameter χ and the vortex viscosity parameter Δ are presented. The results of this parametric study are presented in Figs. 3-14 and Tables 2-4. In all of these results, the aspect ratio of the cavity was fixed at a value of 1.0 (square cavity).

a) Streamlines and temperature contours

Fig. 3 shows the effect of variations of dimensionless time parameter τ on streamlines contours and isotherms contours for the case of strong concentration of microelement $(\chi = 0)$. The intensity of flow activities for each time period is documented by recording the maximum and minimum streamline values. Fig. 3 (a) shows a primary vortex occupying much of the cavity for all the considered time periods. This implies that the fluid is well mixed. When $\tau = \pi/2$, there is a huge clockwise circular cells formed inside the cavity. The maximum value of stream function is zero and the minimum value is $\psi_{\min} = -0.17$. As the time parameter τ decreases to the value $\tau = \pi/6$, the minimum value of stream function increases to the value $\psi_{\min} = -0.08$ and there is a single anti-clock-wise circular contour line formed beside the bottom right corner of the cavity with $\psi_{\max} = 5\times10^{-4}$. Regarding the isotherms contours, the isotherms are accordingly clustered close to the bottom wall, which points out to the existence of high temperature gradients in the vertical direction. In addition, the flow circulation strengthens which facilitates augmentation of heat transfer process. This manifests that convection heat transfer has become the primary energy carrier in this case, so the area which covered by the isotherms contours decreases when the dimensionless time parameter decreases. Note that decreasing the time parameter leads to decreases in the flow circulation.

Fig. 4 shows a comparison between the behaviors of streamlines contours and isotherms contours in the case of strong concentration of microelement which is represented by $\chi = 0$ and the case of weak concentration of microelement which is represented by $\chi = 0.5$ for a fixed value of the time parameter. It is clear that there are two clockwise and anti-clockwise circular cells formed inside the cavity with $\psi_{\max} = 6\times10^{-4}$ and $\psi_{\min} = -0.038$ when $\chi = 0$. Also, the intensity of the fluid activities increases beside the top wall (lid-driven wall). But when $\chi = 0.5$, the intensity of the fluid activities increases beside the bottom wall and there are two clockwise and anti-clockwise circular cells formed with $\psi_{\max} = 0.095$ and $\psi_{\min} = -0.03$. Moreover, the isotherms contours have slight differences between the case of $\chi = 0$ and the case of $\chi = 0.5$. These differences are clearly shown in Figure 7 (b). The area which is covered by isotherms lines in the case of $\chi = 0.5$ is bigger than that for

the case of $\chi = 0$ which means that the fluid for the case of $\chi = 0.5$ is hotter than that for the case of $\chi = 0$.

The effect of the Reynolds number Re on the contours of streamlineas and temperature is shown in Fig. 5. It is found that, the fluid motion becomes more active by increasing the Reynolds number Re and the maximum value of streamfunction increases from $\psi_{\max} = 0$ when $\mathrm{Re} = 50$ to the value $\psi_{\max} = 0.01$ when $\mathrm{Re} = 200$. Howevere, the fluid temperature decreases by increasing the Reynolds number Re and this can be easly seen from the area which is covered by the isotherm contours which decrease due to increasing the Reynolds number Re.

The steady state conditions of this discussion ($\omega\tau = 2\pi$) are investigated in Figs. 10 and 11 and Table 4 which shows the effect of the vortex viscosity parameter Δ on the streamlines contours , isotherms contours, Nusselt number at the bottom wall and values of the average Nusselt number at the bottom and top walls. We should note that there is no lid-driven wall in this case i.e ($U = 0$ *at* $Y = 1$). For a Newtonian fluid ($\Delta = 0$), there are three anti-clockwise and clockwise circular cells formed inside the enclosure with $\psi_{\max} = 0.09$ and $\psi_{\min} = -0.015$. However, for a non-Newtonian micropolar fluid ($\Delta = 2.0$) there are two clockwise and anti-clockwise circular cells inside the cavity with $\psi_{\max} = 0.05$ and $\psi_{\min} = -0.006$. Regarding the isotherms contours, it is seen that these contours cover the whole of the cavity for a Newtonian fluid ($\Delta = 0$) and they are more asymptotic than in the case of a non-Newtonian micropolar fluid ($\Delta = 2.0$).

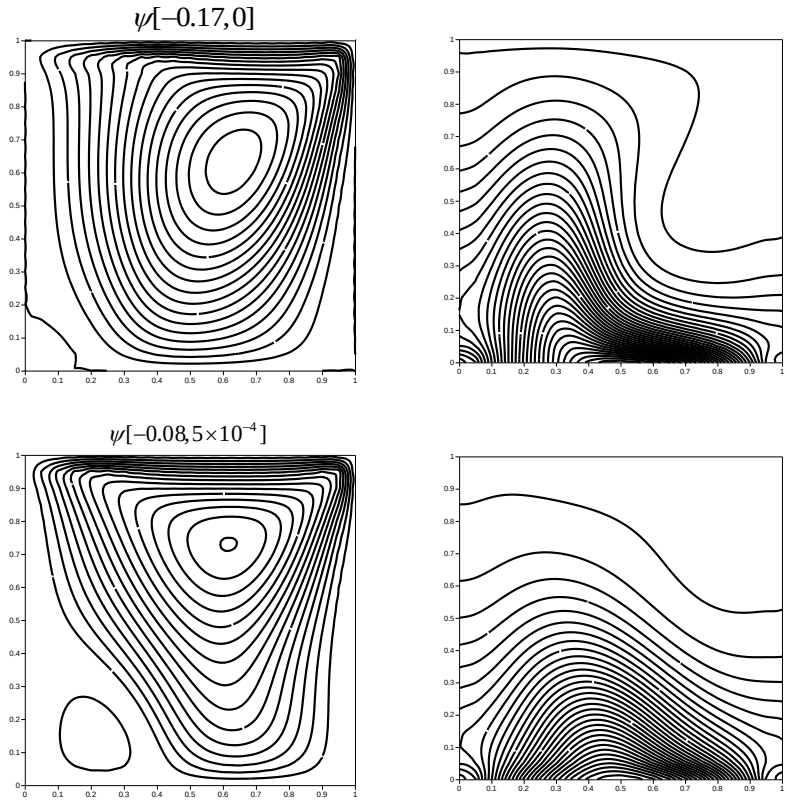

Figure 3. Contours of Streamlines (left) and temperature (right) at $\tau = \pi/2, \pi/6.$(decreasing from top towards bottom).

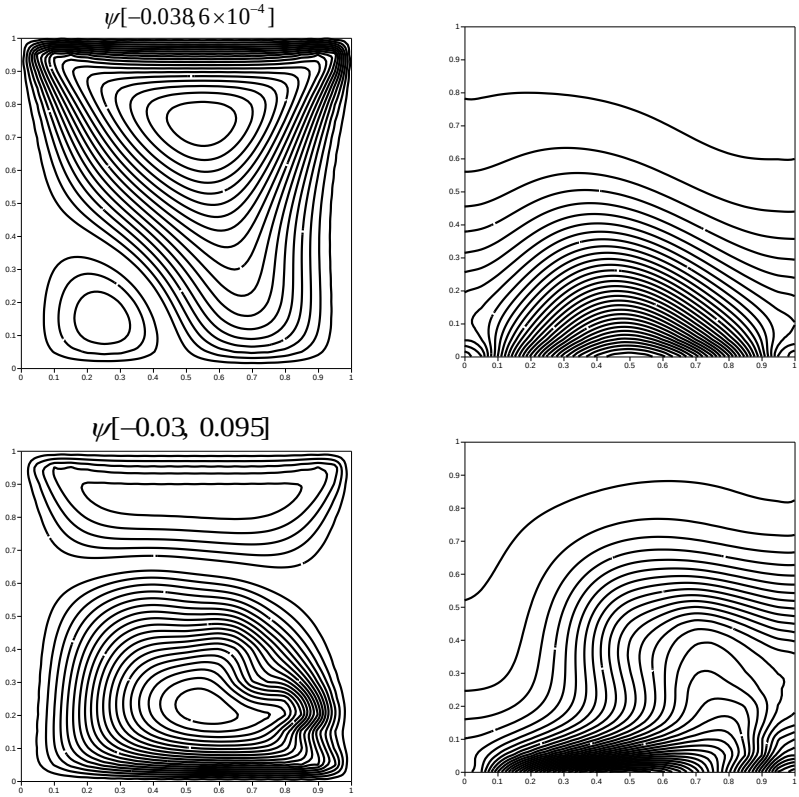

Figure 4. Contours of Streamlines (left) and temperature (right) at $\chi = 0, 0.5.$ (Increasing from top towards bottom).

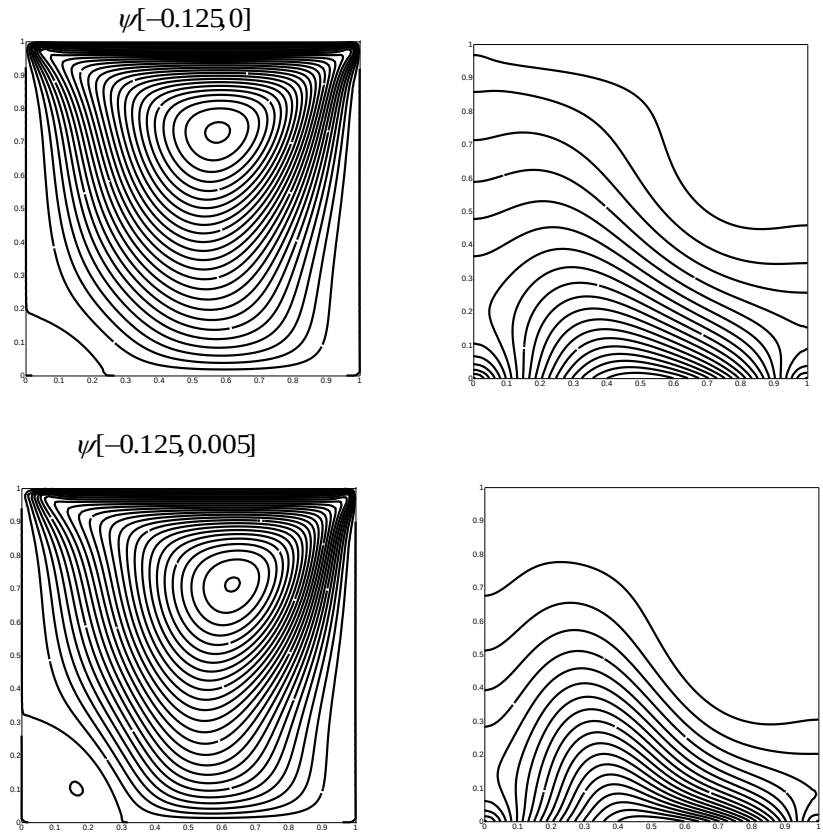

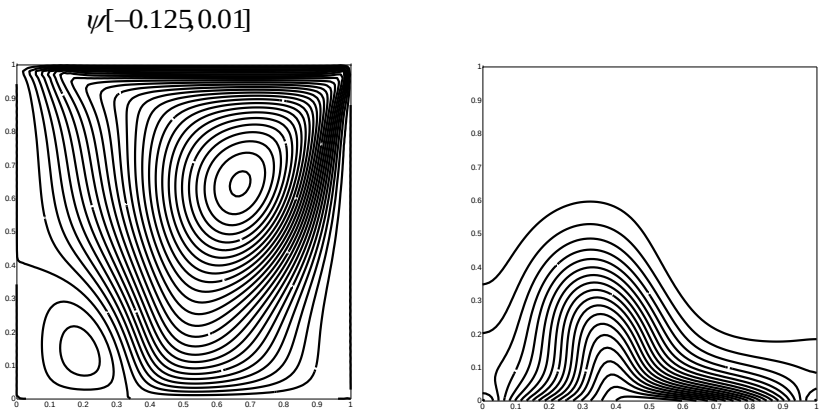

Figure 5. Contours of Streamlines (left) and temperature (right) at $\mathrm{Re} = 50, 100, 200$. (Increasing from top towards bottom).

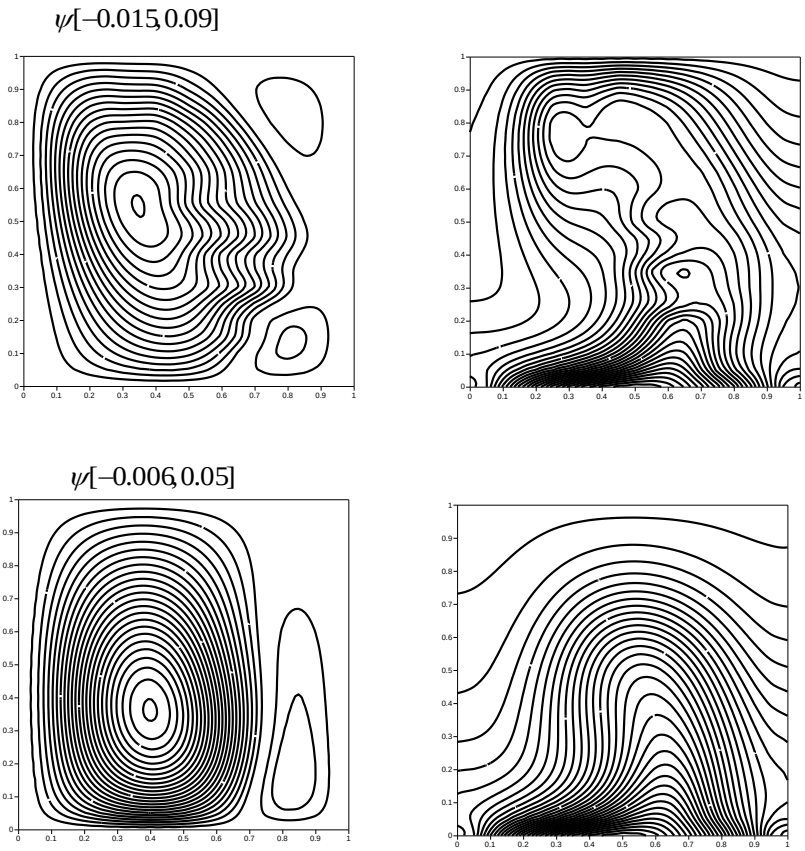

Figure 6. Contours of Streamlines (left) and temperature (right) at $\Delta = 0, 0.5$ (Increasing from top towards bottom).

b) Horizontal and angular velocity components at the enclosure mid section

Figures 7-9 display the effect of the time period ($\omega\tau = \pi/2, \pi/6, \pi$), Reynolds number Re, and the micro-gyration bounday condition parameter χ on the horizontal velocity component at the enclosure mid-section. It is clear that the horizontal velocity component depends strongly on the values of the time period. So, the larger values of U can be achieved when $\omega\tau = \pi/2$ and this agrees with the boundary conditions of the problem. In addition, increases in both the Reynolds number Re and the micro-gyration boundary conditions parameter χ lead to increases in the velocity component U.

Figure 10 shows the effect of the time period ($\omega\tau = \pi/2, \pi/6, \pi$) on the angular velocity component at the enclosure mid-section. The results show that the angular velocity component decreases with increasing values of the time period.

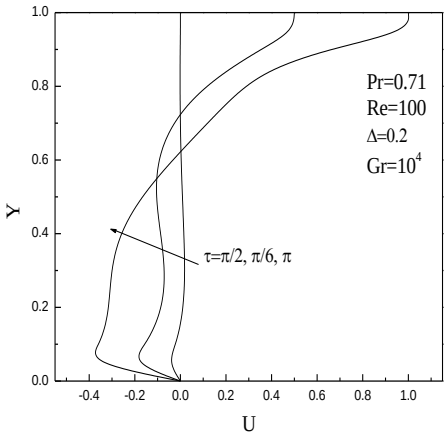

Figure 7. Horizontal velocity component for different values of dimensionless time parameter

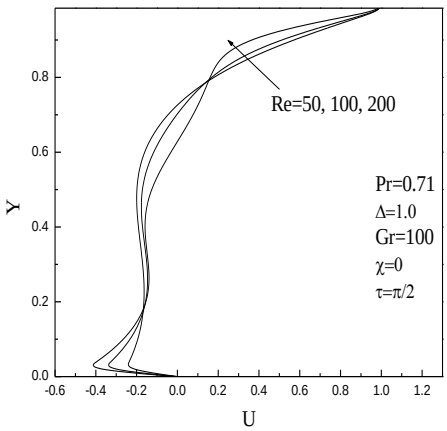

Figure 8. Horizontal velocity component for different values of dimensionless time parameter

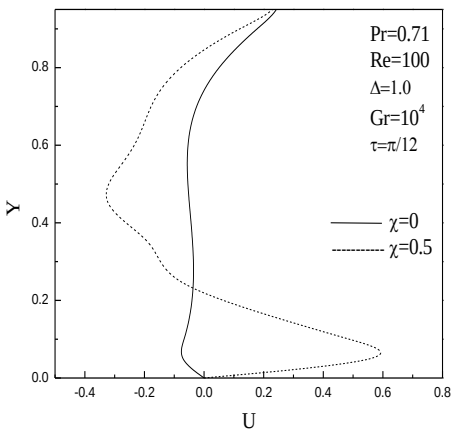

Figure 9. Horizontal velocity component at the enclosure mid-section for different values of micro-gyration boundary conditions parameter

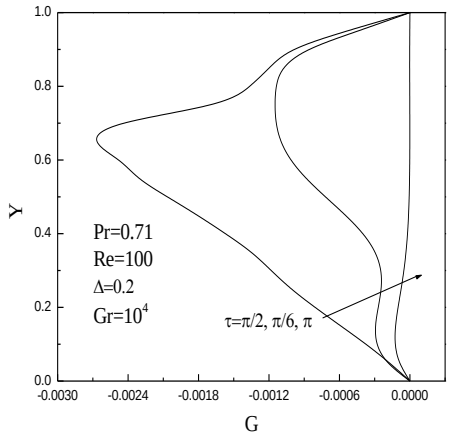

Figure 10. Angular velocity profiles for different values of dimensionless time parameter

c) Nusselt number and average Nusselt number at the top and bottom walls of the cavity

Figures 11-14 depict the effects of the time period ($\omega\tau = \pi/2, \pi/6, \pi$), Reynolds number Re, micro-gyration boundary condition parameter χ and the vortex viscosity parameter Δ on the Nusselt number at the enclosure bottom wall. The results show that, in general, the Nusselt number curves take a a wave-like behavior, which also agrees with the variation of the boundary conditions. In addition, increasing the Reynolds number and the micro-gyration boundary condition parameter causes reductions in the values of the Nusselt number whereas increasing the value of the vortex viscosity parameter results in a decrease in the Nusselt number at the bottom wall.

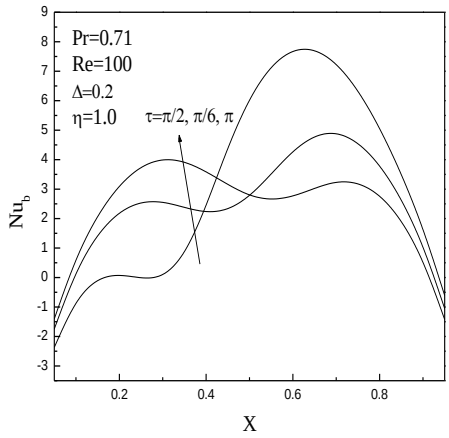

Figure 11. Nusselt number at the bottom wall of the cavity for different values of dimensionless time parameter

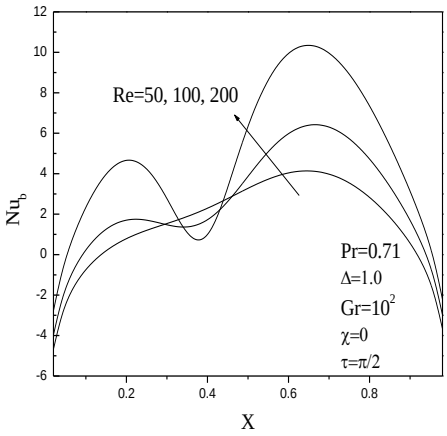

Figure 12. Nusselt number at the bottom wall of the cavity for different values of Reynolds number

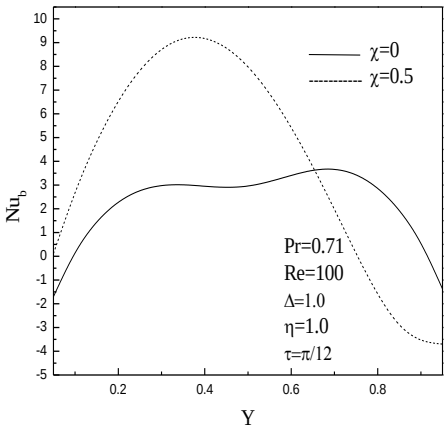

Figure 13. Nusselt number at the enclosure bottom wall for different values of micro-gyration boundary conditions parameter

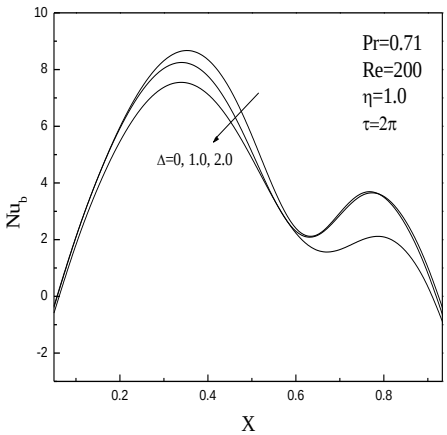

Figure 14. Nusselt number at the enclosure bottom wall for different values of vortex-viscosity parameter

Tables 2-4 show the effects of the time period ($\omega\tau = \pi/2, \pi/6, \pi$), micro-gyration boundary condition parameter χ and the vortex viscosity parameter Δ on the values of the average Nusselt number at the bottom and top walls. As expected, the values of the average Nusselt number at the top and bottom walls of the cavity increase with increasing values of the time parameter. But further increase in the time period ($\omega\tau = \pi$) leads to opposite behaviors. In addition, increasing the value of χ leads to increases in the average Nusselt number at the bottom and top walls whereas the values of average Nusselt number at the enclosure bottom and top walls decreases with increasing vortex viscosity parameter.

Table 2. Values of average Nusselt number at the bottom and the top wall of the cavity for different values of dimensionless time parameter

τ	$\overline{Nu}_b$	$\overline{Nu}_T$
$\pi/6$	2.412021	0.034337
$\pi/2$	2.988618	0.1584773
π	2.358781	0.0123977

Table 3. Values of average Nusselt number at the bottom and the top wall of the cavity for different values of micro-gryation boundary conditions parameter

χ	$\overline{Nu}_b$	$\overline{Nu}_T$
0	2.188595	0.0177269
0.5	3.823426	0.0400139

Table 4. Values of average Nusselt number at the bottom and the top wall of the cavity for different values of vortex-viscosity parameter

Δ	$\overline{Nu}_b$	$\overline{Nu}_T$
0	4.146658	1.451407
1.0	3.999954	0.5383129
2.0	3.389405	0.1446074

5. CONCLUSION

In the present paper, the problem of unsteady mixed convection of a micropolar fluid inside a lid-driven cavity under different micro-gyration boundary conditions was studied. The finite-difference method was employed for the solution of the problem. Comparisons with previously published work on special cases of the problem were performed and found to be in good agreement. Graphical and tabular results for various parametric conditions were presented and discussed. From this investigation, we can draw the following conclusions:

I. In general, the rate of fluid motion and heat characteristics increased by increasing the dimensionless time parameter.
II. A faster motion in the cavity was predicted when the case of weak concentration of microelement

was considered and a weak rate of flow was obtained when the case of strong concentration of microelement was considered.

III. Increasing the micro-gyration boundary conditions parameter led to increases in the average Nusselt number at the bottom and top walls.

IV. Increasing the vortex viscosity parameter led to decreases in both of the rate of fluid motion and heat transfer characteristics.

List of Symbols

B	material parameter
c_p	specific heat of the fluid
g	gravitational acceleration
Gr	Grashof number
j	micro-inertia
l	length of the cavity wall.
N	dimensionless angular velocity
Nu	Nusselt number
P	dimensionless pressure
Pr	Prandtl number
Re	Reynolds number
t	time
T	dimensional temperature
u, v	dimensional velocity components
U, V	dimensionless velocity components
x, y	dimensional coordinates
X, Y	dimensionless coordinates

Greek symbols

β	thermal expansion coefficient
Δ	vortex viscosity parameter
γ	spin gradient viscosity
Ω	vorticity
χ	micro-gyration boundary condition parameter
λ	microrotation parameter
υ	kinamatic viscosity
σ	dimensional angular velocity
θ	dimensionless temperature
ψ	dimensionless stream function

Subscript

0	cold
w	condition on the wall

6. REFERENCES

[1]. A. Eringen, Simple microfluids, Int. J. Eng. Sci., vol. 2, pp. 205-217, 1964.

[2]. A. Eringen, Theory of micropolar fluids, J. Math. Mech., vol.16, pp. 1-18, 1966.

[3]. A. Eringen, Theory of thermomicropolar fluids, J. Math. Anal. Appl., vol. 9, pp. 480-496, 1972.

[4]. Y.Y. Lok, N. Amin, I. Pop, P. Phang, Unsteady boundary layer flow of a micropolar flow near the forward stagnation point of a plane surface, Int. J. Engineering science, vol. 41, pp. 173-186, 2003.

[5]. Y.Y. Lok, N. Amin, I. Pop, Unsteady boundary layer flow of a micropolar flow near the rear stagnation point of a plane surface, Int. J. Thermal sciences, vol. 42, pp. 995-1001, 2003.

[6]. M. M. Abd-Elaziz, Sameh E. Ahmed, Group solution for unsteady boundary layer flow of a micropolar fluid near the rear stagnation point of a plane surface in a porous medium, Laitin Amer. Appl. Res, vol. 38, pp. 161-168, 2008.

[7]. M.A. Mansour, I.M. Hassanien, A.A. Arafa, Combined heat and mass transfer in natural convection flow on a vertical cylinder in a micropolar fluid, Mèca. Appl., vol. 36, pp. 33-47, 1991.

[8]. T. Hsu, P. Hsu, S. Tsai, Natural convection of micropolar fluids in an enclosure with heat sources, Int. J. Heat Mass Transfer. vol. 40, pp. 4239-4249, 1997.

[9]. T. Hsu S. Wang, Mixed convection of micropolar fluids in a cavity, Int. J. Heat Mass Transfer, vol. 43, pp. 1563-1572, 2000.

[10]. A.K. Abdul Hakeem, S. Saravanan, P. Kandaswamy, Buoyancy convection in a square cavity with mutually orthogonal heat generating baffles, Int. J. Heat and Fluid Flow vol. 29 , pp. 1164-1173, 2008.

[11]. P. Kandaswamy, Jinho Lee, A.K. Abdul Hakeem, S. Saravanan, Effect of baffle–cavity ratios on buoyancy convection in a cavity with mutually orthogonal heated baffles, Int. J. Heat Mass Transfer, vol. 51, pp. 1830-1837, 2008.

[12]. R. Bennacera, H. Bejia, A.A. Mohamad, Double diffusive convection in a vertical enclosure inserted with two saturated porous layers confining a fluid layer, Int. J. Ther. Scie. vol. 42, pp. 141–151, 2003.

[13]. T.W. Tong, E. Subramanian, Natural convection in rectangular enclosures partially filled with a porous medium, Int. J. Heat Fluid Flow, vol. 7, pp. 3–10, 1986.

[14]. C. Beckermann, S. Ramadhyani, R. Viskanta, Natural convection flow and heat transfer between a fluid layer and a porous layer inside a rectangular enclosure, J. Heat Transfer, vol. 109, pp. 363–370, 1987.

[15]. C. Beckermann, R. Viskanta, S. Ramadhyani, Natural convection in vertical enclosures containing simultaneously fluid and porous layers, J. Fluid Mech. vol. 186, pp. 257–284, 1988.

[16]. S.B. Sathe, W.-Q. Lin, T.W. Tong, Natural convection in enclosures containing an insulation with a permeable fluid- porous interface, Int. J. Heat Fluid Flow, vol. 9, pp. 389–395, 1988.

[17]. P. Le Breton, J.P. Caltagirone, E. Arquis, Natural convection in a square cavity with thin porous layers on its vertical walls, J. Heat Transfer, vol. 113, pp. 892–899, 1991.

[18]. H. Soh, J.W. Goodrich, Unsteady solution of incompressible Navier–Stokes equations, J.Comput. Phys, vol. 79, pp. 113–134, 1988.

[19]. R.I watsu, J.M. Hyun, K. Kuwahara, Numerical simulation of flows driven by a torsionally

oscillating lid in a square cavity, J. Fluids Engrg, vol. 114, pp. 143–151, 1992.

[20]. R.I. watsu, J.M. Hyun, K. Kuwahara, Convection in a differentially- heated square cavity with atorsionally-oscillating lid, Int. J. Heat Mass Transfer, vol. 35, pp. 1069–1076, 1992.

[21]. K.M. Khanafer, A.M. Al-Amiri, I. Pop, Numerical simulation of unsteady mixed convection in a driven cavity using an externally excited sliding lid, Eur. J. Mech.B/Fluids, vol. 26, pp. 669–687, 2007.

[22]. A.M. Al-Amiri, Analysis of momentum and energy transfer in a lid-driven cavity filled with a porous medium, Int. J. Heat Mass Transfer, vol. 43, pp. 3513–3527, 2000.

[23]. P.M. Gresho, R.L. Lee, R.L. Sani, On the time-dependent solution of the incompressible Navier–Stokes equations in two and three dimensions, in: Recent A dv. Numerical Methods in Fluids, Pineridge, Swansea, UK, 1980.